Antimicrobial evaluation of neutral and cationic iridium(III) and rhodium(III) aminoquinoline-benzimidazole hybrid complexes

European Journal of Medicinal Chemistry 206 (2020) 112694

Contents lists available at ScienceDirect

European Journal of Medicinal Chemistry

journal homepage: http://www.elsevier.com/locate/ejmech

Antimicrobial evaluation of neutral and cationic iridium(III) and rhodium(III) aminoquinoline-benzimidazole hybrid complexes☆

Nadia Baartzes [a], Audrey Jordaan [b], Digby F. Warner [b, c], Jill Combrinck [d], Dale Taylor [e], Kelly Chibale [a, f], Gregory S. Smith [a, *]

[a] Department of Chemistry, University of Cape Town, Rondebosch, 7701, Cape Town, South Africa
[b] SAMRC/NHLS/UCT Molecular Mycobacteriology Research Unit, DST/NRF Centre of Excellence for Biomedical TB Research, Department of Clinical Laboratory Sciences, University of Cape Town, Rondebosch, 7701, Cape Town, South Africa
[c] Wellcome Centre for Infectious Diseases Research in Africa, University of Cape Town, Rondebosch, 7701, South Africa
[d] Division of Clinical Pharmacology, Department of Medicine, University of Cape Town, Observatory, 7925, Cape Town, South Africa
[e] Drug Discovery and Development Centre (H3D), Division of Clinical Pharmacology, Department of Medicine, University of Cape Town, Observatory 7925, Cape Town, South Africa
[f] South African Medical Research Council, Drug Discovery and Development Research Unit, Department of Chemistry and Institute of Infectious Disease and Molecular Medicine, University of Cape Town, Rondebosch 7701, South Africa

ARTICLE INFO

Article history:
Received 23 May 2020
Received in revised form
21 July 2020
Accepted 22 July 2020
Available online 5 August 2020

Keywords:
Bioorganometallic chemistry
Aminoquinolines
Benzimidazoles
Hybrids
Platinum group metals
Antimicrobial

ABSTRACT

A series of neutral and cationic Ir(III) and Rh(III) aminoquinoline-benzimidazole hybrid complexes were synthesised and their inhibitory activities evaluated against *Plasmodium falciparum* and *Mycobacterium tuberculosis*. In general, the hybrid complexes display good activity against the chloroquine-sensitive NF54 strain of *P. falciparum*. The neutral Ir(III)- and Rh(III)-Cp* complexes were the most active (IC_{50} = 0.488 μM for Ir^{III}), maintaining activity against the multidrug-resistant K1 strain. Low to no cytotoxicity against the Chinese hamster ovarian cell line was observed for the tested complexes. Selected active hybrid complexes demonstrated significant inhibition of β-haematin formation in a cell-free NP-40 assay, suggesting an effect on the host haemoglobin degradation pathway as a potential contributing mechanism of action. When tested against *M. tuberculosis* H37Rv, most hybrid complexes displayed moderate to good activity. Again, the neutral complexes outperformed the cationic complexes, with the neutral Ir(III)-Cp* complexes proving most active (MIC_{90} = 0.488−1.490 μM).

1. Introduction

Malaria and tuberculosis (TB) are life-threatening infectious diseases which remain prevalent and are exacerbated by the emergence of resistance to current effective treatments. Malaria, which caused approximately 405 000 deaths in 2018 [1], is caused by *Plasmodium* parasites and transmitted by the female *Anopheles* mosquito vector. The current widely-used treatment is artemisinin-based combination therapy (ACT) which utilises an artemisinin derivative in combination with another antimalarial with a different mechanism of action and longer half-life [2]. Although the ACT regimen is the most efficacious antimalarial treatment, ACT-resistance has been reported in parts of Asia [3,4]. On the other hand, tuberculosis (TB), which resulted in 1.5 million deaths in 2018, is caused by *Mycobacterium tuberculosis* [5]. Treatment of drug-susceptible TB requires a four-drug regimen of first-line drugs; isoniazid, rifampicin, pyrazinamide and ethambutol [6]. Second-line drugs such as fluoroquinolones are used to treat multidrug-resistant TB. The much more difficult to treat extensively drug-resistant strains of *M. tuberculosis* have been reported [7]. Therefore, new chemotherapeutic strategies are continually required to overcome the emergence of resistant microbes.

Molecular hybridisation, defined in drug discovery as the combination of pharmacophores to produce a new hybrid agent, represents a unique approach to tackling drug-resistant microbes. The hybrid compound may afford improved affinity and efficacy compared to the individual parent compounds, through enhanced uptake and additional modes of action [8–10]. Drug resistance may be bypassed through the optimisation of the bioactive components, as well as the physical and chemical properties of the hybrid [8,10].

☆ † CCDC 2002515 contains crystallographic data for compound **6b**.

* Corresponding author.
E-mail address: gregory.smith@uct.ac.za (G.S. Smith).

https://doi.org/10.1016/j.ejmech.2020.112694
0223-5234/

Hybrids incorporating various classes of organic antimalarial pharmacophores have been widely explored in antimalarial studies [11–14]. The strategy of organometallic derivatisation has also garnered significant attention in medicinal chemistry. In this regard ferroquine, a ferrocenyl-aminoquinoline antimalarial currently in Phase IIb combination studies, represents a landmark discovery [15,16]. Literature examples of metal-containing hybrid complexes utilised in antimicrobial studies include trioxaferroquines, reported by Bellot *et al.* [17]. These hybrids, incorporating a 1,2,4-trioxane moiety and ferroquine, display potent activity against CQR strains of *P. falciparum* [17]. Examples of antimicrobial PGM-containing hybrid complexes were reported by Chellan *et al.* [18]. The cationic Ir(III) and Rh(III) complexes of quinoline-sulfadoxine hybrids were active against strains of both *P. falciparum* and *M. tuberculosis* [18].

Previous work within our research group, aimed at targeting drug-resistant parasites, utilised various PGMs and organic scaffolds [19]. Notably, the complexes incorporating metals such as Ru(II), Ir(III) and Rh(III), utilising heterocyclic scaffolds such as quinolines [20–22], benzothiazoles [23] and benzimidazoles [24], gave rise to compounds with favourable activity against drug-sensitive and resistant *P. falciparum* strains. As a prerequisite study to the work presented herein, we previously reported on the antiplasmodial and antimycobacterial evaluation of bioisosteric organic and ferrocenyl aminoquinoline-benzimidazole hybrids [25]. This study explores the incorporation of PGMs into an aminoquinoline-benzimidazole hybrid scaffold, and the effect of the metal and complex charge on antimicrobial activity. The synthesis and characterisation of neutral and cationic Ir(III) and Rh(III) hybrid complexes are reported. Their activities were evaluated against sensitive and resistant strains of *P. falciparum* and the laboratory strain, *M. tuberculosis* H37Rv. The potential of the complexes to inhibit β-haematin formation was also explored.

2. Results and discussion

2.1. Synthesis and characterisation

The 1,2-diamine aminoquinoline precursors (**1a** – **1c**) and 2-phenyl aminoquinoline-benzimidazole hybrids (**2a** – **2c**) were prepared according to published methods [25]. The 2-pyridyl aminoquinoline-benzimidazole hybrids (**3a** – **3c**) were synthesised in an analogous way to compounds **2a** – **2c**. Briefly, compounds **1a** – **1c** were reacted with 2-pyridylcarboxaldehyde in the presence of trifluoroacetic acid and anhydrous magnesium sulfate, to afford compounds **3a** – **3c** *via* cyclo-condensation. Neutral *C^N*-coordinated Ir(III) and Rh(III) complexes (**4a** – **4c** and **5a** – **5c**) were prepared by reacting the 2-phenyl hybrid ligands with metal dimers, *via* C–H activation. Compounds **2a** – **2c** were reacted with sodium acetate and pentamethylcyclopentadienyliridium(III) chloride dimer in dichloromethane and ethanol at room temperature. This afforded the cyclometalated Ir(III) complexes (**4a** – **4c**) as dull yellow powders in moderate yields (52–63%). On the other hand, successful synthesis of the cyclometalated Rh(III) complexes required higher reaction temperatures, as reactions at room temperature afforded product mixtures with a low proportion of the desired product. Thus, compounds **2a** – **2b** were reacted with sodium acetate and pentamethylcyclopentadienylrhodium(III) chloride dimer in dichloromethane and methanol at 65 °C. The desired cyclometalated Rh(III) complexes (**5a** – **5b**) were isolated as dull orange powders in low to moderate yields (36–47%). Cationic *N^N*-coordinated Ir(III) and Rh(III) complexes were prepared *via* successive bridge-splitting and counter-ion exchange reactions. In a one-pot synthesis, compounds **3a** – **3c** were reacted with either $[Ir(Cp^*)Cl_2]_2$ or $[Rh(Cp^*)Cl_2]_2$ in dichloromethane and ethanol at room temperature. This was followed by counter-ion exchange using ammonium hexafluorophosphate in ethanol at 0 °C. These reactions afforded the desired cationic Ir(III) complexes (**6a** – **6c**) as yellow powders in moderate to good yields (53–71%), while the Rh(III) complexes (**7a** – **7c**) were isolated as orange powders in high yields (70–83%). The overall synthetic route is shown in Scheme 1.

Successful synthesis of the precursors, hybrid ligands and PGM-containing hybrid complexes was confirmed using ^{1}H and ^{13}C{^{1}H} NMR spectroscopy, IR spectroscopy and electrospray ionisation (ESI) mass spectrometry. The characterisation data of compounds **1a** – **1c** and **2a** – **2c** are in agreement with the reported literature data [25]. For compounds **3a** – **3c**, cyclo-condensation to form the 2-pyridylbenzimidazole is evident in the ^{1}H NMR spectra. In addition to the signals for the quinoline and phenyl rings, four signals for the protons of the pyridyl ring appear in the spectra, confirming incorporation of the 2-pyridyl moiety. A lone amine proton signal is present in the spectra, where there were two in the 1,2-diamine precursors (**1a** – **1c**). As reported for the 2-phenyl hybrids (**2a** – **2c**), the IR spectra of compounds **3a** – **3c** display one ν(C=N) absorption band (1609–1613 cm^{-1}) corresponding to the overlapping quinoline and benzimidazole imine moieties. The presence of an additional ν(C=N) band (1590–1592 cm^{-1}) for the pyridyl moiety further confirms cyclisation.

In the ^{1}H NMR spectra of the neutral and cationic complexes (**4**–**7**), successful complexation was indicated by the presence of a singlet (1.6–1.7 ppm) corresponding to the fifteen protons of the pentamethylcyclopentadienyl (Cp*) moiety. Signals corresponding to selected methylene protons appear as multiplets as a result of the chiral metal centre, which brings about diastereotopicity in the propyl linker. For complexes **4a** – **4c** and **5a** – **5b**, signals in the aromatic region of the spectra integrate for one fewer aromatic proton compared to their respective ligands. This confirmed the loss of an aromatic proton as a result of successful cyclometalation *via* C–H activation. The spectra also revealed doubling up of selected proton signals, suggesting the presence of conformational isomers in solution. This was confirmed by conducting NMR studies at an elevated temperature (60 °C), causing either a significant decrease or complete disappearance of the duplicate signals and suggesting conversion to the more stable conformer. In the ^{1}H NMR spectra of complexes **6a** – **6c** and **7a** – **7c**, all proton signals shift downfield compared to their respective ligands (**3a** – **3c**). This is expected as a result of the positive charge at the metal centre and provides evidence of successful coordination. The positively charged metal centre draws more electron density from the ligand, resulting in the deshielding effect seen in the NMR. The presence of the PF_6^- counter-ion is confirmed by the appearance of a septet around −144 ppm in the ^{31}P{^{1}H} NMR spectra complexes **6a** – **6c** and **7a** – **7c**. In the IR spectra of complexes **4**–**7**, coordination to the metal centre results in shifts in the ν(C=N) absorption bands. For complexes **4**–**5**, the benzimidazole ν(C=N) absorption band shifts to lower wavenumbers compared to the ligands. For complexes **6**–**7**, the benzimidazole ν(C=N) band shifts to lower wavenumbers and the pyridyl ν(C=N) band shifts to higher wavenumbers. The mass spectra of complexes **4**–**5** display base peaks corresponding to the $[M-Cl+H]^{2+}$ fragment, while the spectra of complexes **6**–**7** display base peaks assigned to the $[M+H]^{2+}$, $[M-Cl]^{2+}$ and $[M-Cl+H]^{3+}$ fragments, where M refers to the complex cation without the PF_6^- counter-ion.

2.2. Molecular structure of compound *6b*

Suitable crystals of compound **6b** were obtained and analysed by single-crystal X-ray diffraction. Crystals were grown by slow diffusion of hexane into a solution of compound **6b** in acetone,

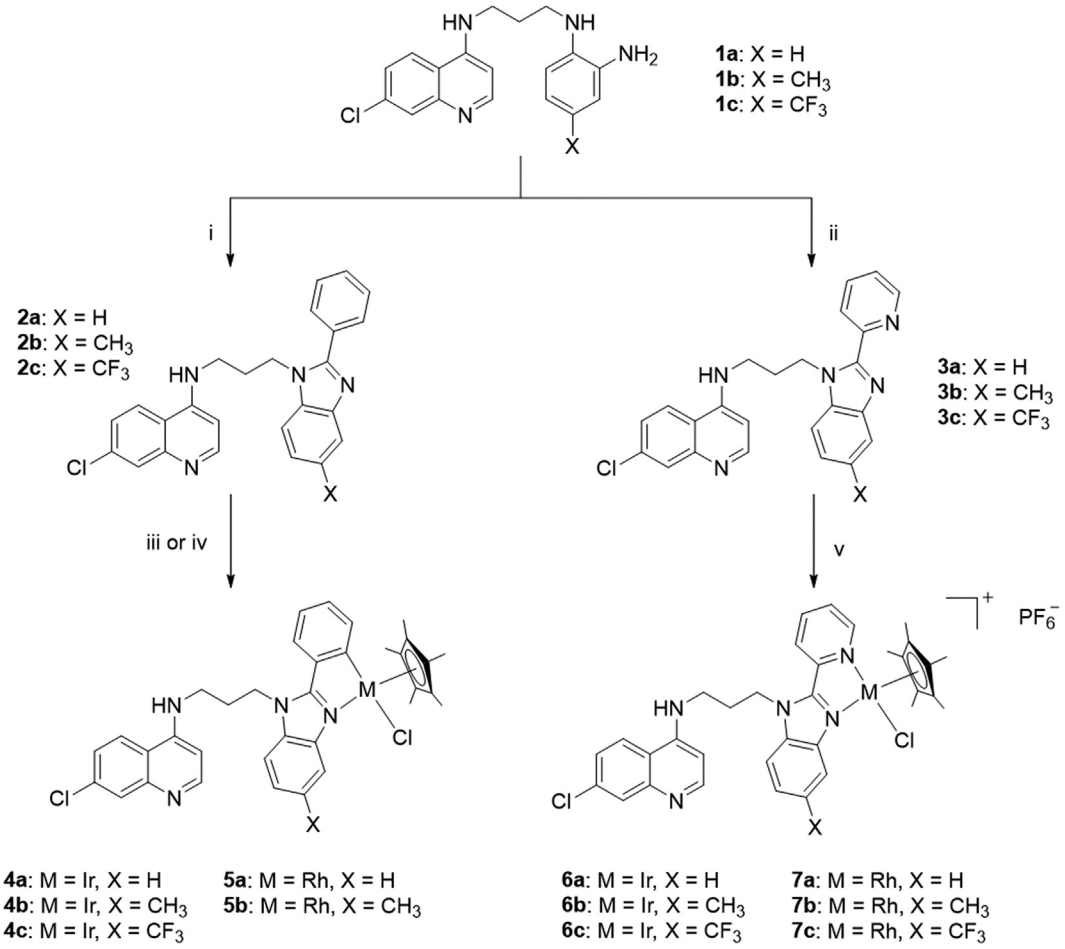

Scheme 1. Synthesis of PGM-containing aminoquinoline-benzimidazole hybrid complexes. Reagents and conditions: (i) benzaldehyde/TFA/$MgSO_4$/EtOH/80 °C/24 h; (ii) 2-pyridinecarboxaldehyde/TFA/$MgSO_4$/EtOH/80 °C/24 h; (iii) $[Ir(Cp^*)Cl_2]_2$/NaOAc/DCM:EtOH/25 °C/24 h; (iv) $[Rh(Cp^*)Cl_2]_2$/NaOAc/DCM:MeOH/65 °C/96 h; (v) $[Ir(Cp^*)Cl_2]_2$ or $[Rh(Cp^*)Cl_2]_2$/DCM:EtOH/25 °C/16–24 h, NH_4PF_6/0 °C/2 h.

forming red block crystals in a monoclinic crystal system with the $P2_1/n$ space group. The molecular structure of compound **6b** is shown in Fig. 1 and confirms the desired structure of compound **6b**. The 2-pyridylbenzimidazole ligand coordinates in a bidentate-chelating manner, through the benzimidazole- and pyridyl-nitrogen donor atoms. In addition, the presence of the cationic *N^N*-coordinated Ir(III) complex is further confirmed by the presence of the hexafluorophosphate counter-ion in the molecular structure. The complex adopts a pseudo-tetrahedral geometry around the iridium metal centre. This three-dimensional shape, described as a 'piano-stool' geometry, is commonly adopted by half-sandwich complexes.

Selected bond lengths and angles are listed in Table 1. The Ir–Cp* bond distances range between 1.339 and 1.467 Å. The Cl–Ir–N_1 and Cl–Ir–N_2 bond angles are comparable, at the near orthogonal 86.06 and 85.88°, respectively, while the N–Ir–N bond angle is significantly smaller (75.72°). These bond angles are in agreement with previously reported *N^N*-coordinated Ir(III), Rh(III) and Ru(II) complexes, which are structurally similar [26–28]. The Ir–Cl and Ir–N_{pyr} bond lengths of complex **6b** are comparable, with distances of 1.594 and 1.587 Å, respectively. The Ir–N_{imine} bond length is shorter, measuring at 1.349 Å. Although the geometry and bond angles about the metal centre correlate well with analogous complexes in the literature, the metal-ligand bond lengths in the molecular structure of complex **6b** are significantly shorter than corresponding bond lengths reported. Analogous M–$N_{imine/pyr}$ lengths are approximately 2.1 Å, while M – Cl lengths are approximately 2.4 Å in the literature [26,27].

2.3. In vitro antiplasmodial evaluation and cytotoxicity

The neutral *C^N*-coordinated and cationic *N^N*-coordinated Ir(III) and Rh(III) complexes were evaluated for their *in vitro* antiplasmodial activity using the *Plasmodium* lactate dehydrogenase (pLDH) assay [29]. Compounds were screened against the chloroquine-sensitive (CQS) NF54 and multidrug-resistant (MDR) K1 strain of *P. falciparum*. Chloroquine (CQ) was used as the control drug in the screening. The IC_{50} values and resistance indices (RI) are summarised in Table 2.

In general, most of the ligands (**3a** – **3c**) and PGM-containing hybrid complexes (**4**–**7**) display good antiplasmodial activity against the CQS NF54 strain, with IC_{50} values in the low micromolar range. It is noteworthy that the most active ligands, neutral and cationic complexes are the trifluoromethyl-substituted analogues (**2c**, **3c**, **4c**, **6c** and **7c**), which have IC_{50} values of 0.431, 0.410, 0.488, 1.454 and 0.194 μM, respectively. Contrasting trends are observed for the activity of the Ir(III) complexes versus the Rh(III) complexes. In the case of the neutral complexes, the unsubstituted Ir(III) complex **4a** (2.007 μM) is less active than the corresponding Rh(III) complex **5a** (1.073 μM), while the methyl-substituted complexes **4b** and **5b** have comparable activity (1.676 and 1.327 μM). For the cationic complexes, the unsubstituted and methyl-substituted

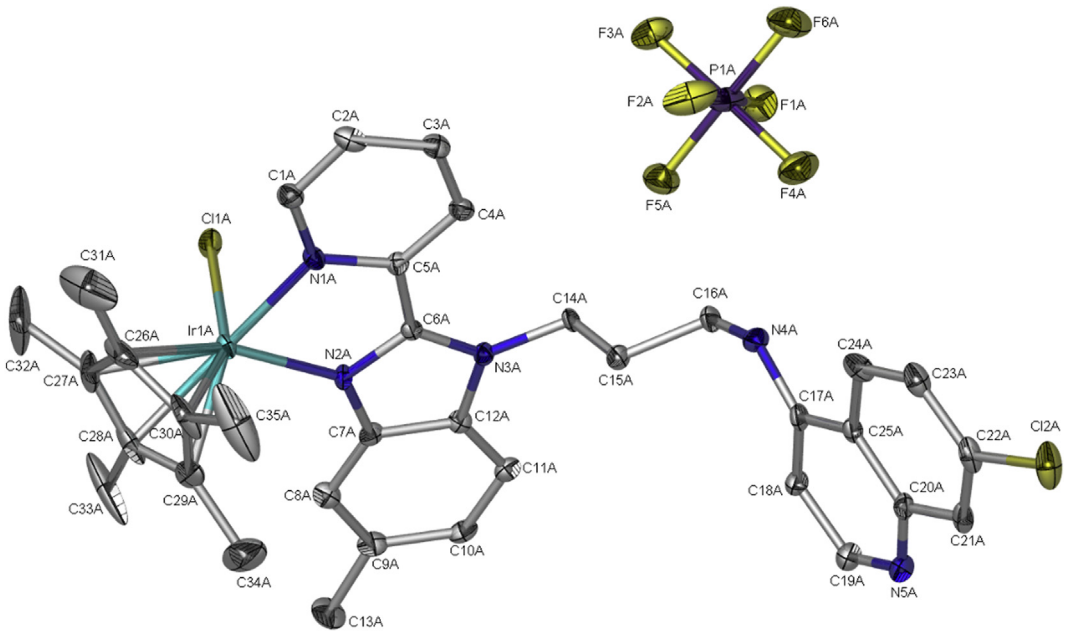

Fig. 1. Molecular structure of compound **6b**, with ellipsoidal models drawn at the 40% probability level.

Table 1
Selected bond lengths and angles of compound **6b.**

	6b
Bond lengths (Å)	
Ir(1A) – Cl(1A)	1.594(4)
Ir(1A) – N(1A)	1.587(4)
Ir(1A) – N(2A)	1.349(6)
Ir(1A) – C(26A)	1.357(6)
Ir(1A) – C(27A)	1.392(6)
Ir(1A) – C(28A)	1.339(5)
Ir(1A) – C(29A)	1.398(6)
Ir(1A) – C(30A)	1.467(5)
Bond angles (°)	
Cl(1A) – Ir(1A) – N(1A)	86.06(12)
Cl(1A) – Ir(1A) – N(2A)	85.88(12)
N(1A) – Ir(1A) – N(2A)	75.72(14)

Table 2
In vitro antiplasmodial data and resistance indices for compounds **2**–**7** and CQ.

			IC_{50} (μM) ± SE		
Compound	M	X	NF54	K1	RI[b]
2a	–	H	5.553 ± 0.063[a]	0.201 ± 0.003[a]	0.036
2b	–	CH_3	0.784 ± 0.016[a]	0.457 ± 0.095[a]	0.583
2c	–	CF_3	0.431 ± 0.012[a]	0.151 ± 0.004[a]	0.350
3a	–	H	1.089 ± 0.168	>20	–
3b	–	CH_3	4.984 ± 0.613	ND[c]	–
3c	–	CF_3	0.410 ± 0.028	>20	–
4a	Ir	H	2.007 ± 0.075	2.844 ± 0.030	1.417
4b	Ir	CH_3	1.676 ± 0.171	2.181 ± 0.025	1.301
4c	Ir	CF_3	0.488 ± 0.062	0.688 ± 0.032	1.410
5a	Rh	H	1.073 ± 0.028	2.217 ± 0.167	2.066
5b	Rh	CH_3	1.327 ± 0.255	1.810 ± 0.176	1.364
6a	Ir	H	>10	ND[c]	–
6b	Ir	CH_3	>10	ND[c]	–
6c	Ir	CF_3	1.454 ± 0.043	>10	–
7a	Rh	H	2.001 ± 0.148	>10	–
7b	Rh	CH_3	1.867 ± 0.562	>10	–
7c	Rh	CF_3	0.194 ± 0.066	>10	–
CQ	–	–	0.0160 ± 0.0005	0.164 ± 0.018	10.250

[a] Data previously reported [25].
[b] RI = IC_{50}(K1)/IC_{50}(NF54).
[c] ND = not determined.

Ir(III) complexes **6a** and **6b** are inactive (IC_{50} > 10 μM) at the maximum tested concentration. The Rh(III) complexes **7a** – **7c** display significantly enhanced activity, at least 5-fold greater than their corresponding Ir(III) complexes **6a** – **6c**.

Selected hybrid complexes, which were sufficiently active in the NF54 strain ($IC_{50} \leq 2$ μM), were screened against the MDR K1 strain of *P. falciparum*. Compounds **3a**, **3c**, **6c**, **7a** – **7c** are inactive against K1 parasites (IC_{50} > 10 μM) at the tested concentration. The neutral complexes (**4a** – **4c** and **5a** – **5b**) display good antiplasmodial activity in the low micromolar range. In the resistant K1 strain, corresponding unsubstituted and methyl-substituted Ir(III) and Rh(III) complexes (**4a** – **4b** and **5a** – **5b**) are comparably active, giving rise to IC_{50} values in the range 1.810–2.844 μM. Once again, the activity of the analogue with the more hydrophobic CF_3 substituent, compound **7c**, is enhanced, displaying an IC_{50} value of 0.688 μM. Comparing the activity in the CQS NF54 and MDR K1 strain, most of the compounds have comparable or slightly decreased activity in the resistant strain. Compounds **4a** – **4c** and **5a** – **5b** all display resistance indices in the range 1–2 (RI ≥ 1), significantly lower than that of CQ (RI = 10). However, across the sensitive and resistant strains, the hybrid complexes were less active than the control drug, CQ. When comparing the effect of complex charge on the antiplasmodial activity, it should be noted that the neutral cyclometalated Ir(III) and Rh(III) complexes (**4**–**5**) generally outperformed their corresponding cationic complexes (**6**–**7**), in both the sensitive and resistant strains.

Evaluating the effect of organometallic derivatisation on the antiplasmodial activity, the trends observed are not consistent across the different series and *P. falciparum* strains. In the NF54 strain, the neutral unsubstituted Ir(III) and Rh(III) complexes, **4a** and **5a**, are almost 3- and 5-fold more potent than the ligand **2a** (5.553 μM) [25]. Cationic complexes **7b** and **7c** are more active than their respective ligands **3a** (1.089 μM) and **3c** (0.410 μM). Trifluoromethyl-substituted complex **7c** maintains comparable activity to the ligand **2c** (0.431 μM). In all other cases, activity is not maintained upon coordination of the metal moiety, and higher IC_{50} values are observed for the complexes compared to their respective ligands.

As a result of their favourable activity against the NF54 and K1 *P. falciparum* strains, the *C^N*-coordinated Ir(III) and Rh(III) complexes (**4** - **5**) were screened against the non-tumorigenic CHO cell-line, to determine their cytotoxicities and to ascertain selectivity. The compounds were evaluated using the MTT assay [30,31], using emetine as the control drug. The *N^N*-coordinated Ir(III)-Cp* and Rh(III)-Cp* complexes (**6** - **7**) did not maintain activity in the resistant K1 strain and were thus not evaluated against CHO cells. The IC_{50} values and selectivity indices (SI) of the screened compounds are reported in Table 3.

Compound **4c** displays low toxicity towards the CHO cells, giving rise to a moderate micromolar IC_{50} value of 14.14 μM. Compounds **4a** – **4b** and **5a** – **5b** were non-cytotoxic at the highest concentration tested, with IC_{50} values greater than 50 μM. The selectivity indices (SI) were determined to gauge the selectivity of the tested compounds toward the *Plasmodium* strains compared to the CHO cell-line. The SI values were calculated to be greater than 28 and 20 for the sensitive NF54 (SI_1) and resistant K1 (SI_2) strains, respectively. These values, which are significantly greater than one, suggest that the neutral Ir(III) and Rh(III)-containing hybrid complexes are selective toward the *Plasmodium* strains. In addition, it may also imply that the antiplasmodial properties of these complexes can be attributed to mechanisms other than general cytotoxicity.

2.4. β-haematin inhibition activity

The haem degradation pathway, which takes place in the *Plasmodium* digestive vacuole, is an important target of many quinoline-containing antimalarials. Chloroquine and related compounds have been shown to target this pathway. Thus, selected active complexes were evaluated for their ability to interfere with this pathway as a potential contributing mechanism of action. The detergent-mediated NP-40 assay [32] and subsequent colorimetric pyridine ferrihaemochrome method [33] were used to assess the β-haematin (synthetic haemozoin) inhibition ability of the iridium and rhodium complexes of interest. Compounds **3c**, **4a**, **4c**, **5a**, **5b**, **6c**, and **7c** were tested, and CQ was used as the positive control. The IC_{50} values obtained are listed in Table 4.

The hybrid ligand (**3c**) and the PGM-containing hybrid complexes (**4a**, **4c**, **5a**, **5b**, **6c**, and **7c**) were all found to inhibit β-haematin formation in the cell-free assay. In general, the PGM complexes are potent inhibitors, at least 2-fold more active than CQ (73.98 μM). The X substituent appears to have no significant effect on the β-haematin inhibition activity. The cationic *N^N*-coordinated complexes (**6c** and **7c**), were more active than the neutral *C^N*-coordinated complexes (**4**–**5**). The superior activity of the cationic compounds may be the result of their enhanced solubility in the assay medium over time, compared to the neutral compounds. The enhanced solubility may allow greater interaction with the haematin species, which may result in greater β-haematin inhibition. Additionally, the different metals have an effect on the β-haematin inhibition activity, as is evident from the IC_{50} values. The Ir(III)-containing complexes (**4a** and **4c**) display enhanced activity compared to the Rh(III)-containing complexes (**5a** and **5b**). The IC_{50} values of the Ir(III) complexes **4a** and **4c** (13.88–16.03 μM) are approximately two-fold lower than the Rh(III) complexes **5a** and **5b** (31.05–36.34 μM). With regards to the effect of metalation on the β-haematin inhibition activity, contrasting trends are observed. The previously reported activity of ligand **2c** (15.90 μM) [25] is comparable to that of the corresponding Ir(III) complex **4c** (16.03 μM), suggesting a negligible effect of metalation on the activity. On the other hand, complexes **6c** (5.46 μM) and **7c** (8.39 μM) are approximately 10- and 6-fold more active than the ligand **3c** (54.08 μM), suggesting that metalation significantly enhanced β-haematin inhibition for the selected cationic complexes. Furthermore, there is no discernable correlation between β-haematin inhibition activity and the *in vitro* antiplasmodial activity. This may suggest additional contributing mechanisms of action, which affect the overall antiplasmodial activity.

Table 3
Cytotoxicity data and selectivity indices of selected compounds (**4**–**5**) and the control, emetine.

Compound	CHO IC_{50} (μM)	SI_1[a]	SI_2[b]
4a	>50	–	–
4b	>50	–	–
4c	14.14	28.98	20.55
5a	133.30	124.23	60.13
5b	78.89	59.45	43.59
Emetine	0.0181	–	–

[a] $SI_1 = IC_{50}(CHO)/IC_{50}(NF54)$.
[b] $SI_2 = IC_{50}(CHO)/IC_{50}(K1)$.

Table 4
β-haematin inhibition activity of selected hybrid compounds and CQ.

Compound	IC_{50} (μM) [95% confidence interval]
2c	15.90 [15.31 to 16.51][a]
3c	54.08 [51.22 to 57.09]
4a	13.88 [12.13 to 15.88]
4c	16.03 [14.43 to 17.81]
5a	31.05 [30.03 to 32.09]
5b	36.34 [33.63 to 39.28]
6c	5.46 [5.01 to 5.95]
7c	8.39 [7.83 to 8.99]
CQ	73.98 [71.14 to 76.94]

[a] Data previously reported [25].

2.5. In vitro antimycobacterial screening

To the best of our knowledge, literature reports exploring the antimycobacterial properties of PGM-containing hybrid complexes are limited, but do include examples of antimycobacterial Ru(II), Ir(III) and Rh(III)-containing hybrid complexes [18,34]. With this in mind, the *C^N*-coordinated and *N^N*-coordinated Ir(III) and Rh(III) complexes (**4**–**7**) were evaluated for their *in vitro* activities against *M. tuberculosis* H37Rv. Using the broth micro dilution method [35], minimum inhibitory concentration (MIC) values were determined. The 7-day MIC_{90} values for the test compounds and the control, rifampicin, are summarised in Table 5. The compounds were screened using two different growth media, Middlebrook 7H9-ADC (albumin-dextrose complex) and 7H9-CAS (casitone). Similar trends in activity were evident in both media, however greater activity was generally observed in 7H9-CAS.

The 2-pyridyl ligands (**3a** – **3c**) proved inactive at the tested concentration (MIC_{90} > 125 μM). Considering the MIC_{90} values obtained in the 7H9-CAS medium, the PGM-containing hybrid complexes (**4**–**7**), which display moderate to good antimycobacterial activity, are significantly less active than the positive control, displaying MIC_{90} values at least 19-fold greater than the antibiotic rifampicin (0.026 μM). For the neutral complexes, there is no discernable correlation between the antimycobacterial activity and the varying 5-position substituent (X). However, an interesting trend is observed for the cationic complexes. For both the Ir(III) complexes (**6a** – **6c**) and Rh(III) complexes (**7a** – **7c**), incorporation of the hydrophobic substituents (CH_3 and CF_3) results in enhanced activity. The analogues with the more hydrophobic trifluoromethyl group (**6c** and **7c**) have the lowest MIC_{90} values of 31.25 and 17.994 μM, respectively. This trend in activity suggests a correlation

Table 5
Antimycobacterial activity of compounds **2**–**7**.

Compound	Day 7 MIC_{90} (μM) [medium: 7H9 GLU CAS]	Day 7 MIC_{90} (μM) [medium: 7H9 GLU ADC]
2a	50.6[a]	38.8[a]
2b	32.7[a]	>62.5[a]
2c	15.8[a]	89.1[a]
3a	>125	>125
3b	>125	>125
3c	>125	>125
4a	0.488	4.244
4b	1.490	7.813
4c	1.100	3.652
5a	8.778	15.309
5b	8.183	15.800
6a	62.500	>125
6b	39.218	>125
6c	31.250	31.250
7a	31.250	62.500
7b	19.215	47.679
7c	17.994	31.250
Rifampicin	0.026	0.002

between hydrophobicity and the antimycobacterial activity. The link between hydrophobicity and the antimycobacterial activity suggests a possible relationship between lipophilicity and activity. A positive correlation was observed for the antimycobacterial activity of the previously reported aminoquinoline-benzimidazole hybrids [25], which is further supported by recent studies investigating the correlation [36–38].

No conclusive statement can be made on the effect of the different metals (Ir versus Rh) on the antimycobacterial activity, as trends vary. With regards to the neutral complexes, the Ir(III) complexes **4a** – **4c** (0.488–1.490 μM) are significantly more active than the Rh(III) complexes **5a** – **5b** (8.778 and 8.183 μM). In contrast, for the cationic complexes, the Ir(III) complexes **6a** – **6c** (31.250–62.500 μM) are consistently less active than their corresponding Rh(III) analogues **7a** – **7c** (17.994–31.250 μM). Considering the effect of complex charge on the activity, the neutral complexes **4**–**5** significantly outperformed their corresponding cationic complexes **6**–**7**. Furthermore, it is evident that for this series of hybrid ligands and complexes, organometallic derivatisation with the PGMs results in significantly enhanced antimycobacterial activity. In all cases, the Ir(III)- and Rh(III)-containing complexes are more active than the corresponding ligands. The previously reported 2-phenyl hybrid ligands (**2a** – **2c**) display moderate activity (15.8–50.6 μM) and coordination of the metal moiety results in a 4- to 104-fold increase in activity for the neutral complexes (**4a** – **4c** and **5a** – **5b**). While the 2-pyridyl hybrid ligands (**3a** – **3c**) are inactive at the test concentration (MIC_{90} > 125 μM), coordination of the metal gives rise to moderately active cationic complexes (**6a** – **6c** and **7a** – **7c**).

3. Conclusions

A series of 2-phenyl and 2-pyridyl aminoquinoline-benzimidazole ligands and corresponding neutral and cationic Ir(III) and Rh(III) complexes were synthesised and evaluated as antimicrobial agents against *P. falciparum* and *M. tuberculosis* strains. In the CQS NF54 and MDR K1 strains of *P. falciparum*, selected compounds displayed good activity with IC_{50} values in the low micromolar range. The neutral Ir(III)- and Rh(III)-Cp* complexes (**4a** – **4c** and **5a** – **5b**) were most potent overall. While the cationic complexes were inactive against K1 parasites at the tested concentration, the neutral complexes maintained significant activity, displaying RI values equal to or above one (RI ≥ 1). Against non-tumorigenic CHO cells, all tested compounds displayed insignificant cytotoxic effects. In addition, the hybrid complexes were selective toward the *Plasmodium* strains compared to CHO cells, giving rise to selectivity indices significantly greater than one. A 2-pyridyl ligand and selected active hybrid complexes were screened for their potential β-haematin inhibition ability, demonstrating potent inhibitory effects in the cell-free assay.

When evaluated against *M. tuberculosis* H37Rv, most hybrid complexes displayed moderate to good antimycobacterial activity. As seen in the antiplasmodial assay, the neutral Ir(III)- and Rh(III)-Cp* complexes (**4a** – **4c** and **5a** – **5b**) were significantly more active than the cationic Ir(III)- and Rh(III)-Cp* complexes, suggesting that the neutral charge is favourable for both antiplasmodial and antimycobacterial activity. The activity of the cationic complexes showed a positive correlation with the hydrophobicity of the 5-position substituent (H, CH_3, CF_3), suggesting a further link between antimycobacterial activity and lipophilicity. However, this trend was not observed for the neutral complexes. Furthermore, metalation resulted in significantly enhanced antimycobacterial activity of the complexes compared their respective ligands in all cases. This indicates that incorporation of the PGM may be favourable for potent antimycobacterial activity.

4. Experimental

4.1. Materials and methods

All reagents and solvents were purchased from commercial sources (Sigma Aldrich, Combi-blocks, Kimix and Merck). The 1,2-diamine aminoquinoline precursors (**1a** – **1c**) [25], 2-phenyl aminoquinoline-benzimidazole hybrids (**2a** – **2c**) [25] and the metal dimers, $[Ir(Cp^*)Cl_2]_2$ and $[Rh(Cp^*)Cl_2]_2$ [39], were prepared using modified literature methods. Infrared (IR) absorptions were measured on a PerkinElmer Spectrum 100 FT-IR spectrometer using Attenuated Total Reflectance (ATR). Nuclear Magnetic Resonance (NMR) spectra were recorded on a Varian Mercury XR300 MHz (^1H at 300.08 MHz), a Bruker 400 Biospin GmbH (^1H at 400.22 MHz, $^{13}C\{^1H\}$ at 100.65 MHz, $^{31}P\{^1H\}$ at 161.80 MHz) or a Bruker 600 FT spectrometer (^1H at 600.10 MHz, $^{13}C\{^1H\}$ at 150.60 MHz) spectrometer at 30 °C. Chemical shifts are reported using tetramethylsilane (TMS) as the internal standard. Mass spectrometry determinations were carried out using Electron Impact (EI) on a JEOL GC Matell instrument or Electrospray Ionisation (ESI) on a Waters API Quattro Micro triple quadrupole mass spectrometer with data recorded using both the positive and negative modes.

Melting points were determined using a Büchi Melting Point Apparatus B-540. Purity of compounds **3a** − **3c** was determined using an analytical Agilent HPLC 1260 equipped with an Agilent DAD 1260 UV/vis detector and a X Bridge C18 column (2.5 μM, 50 mm × 3 mm). The compounds were eluted using a mixture of solvent A (10 mM NH_4OAc/H_2O) and solvent B (10 mM NH_4OAc/MeOH) at a flow rate of 0.9 mL/min. The gradient elution conditions were as follows: 15% solvent B between 0 and 0.5 min, 15–100% solvent B between 0.5 and 1.2 min, 100% solvent B between 1.2 and 4.5 min. Purity was determined at 280 nm. Compounds **3a** − **3c** were confirmed to have greater than 97% purity.

4.2. General method for synthesis of 2-pyridyl hybrids (**3a** − **3c**)

Compound **1a**, **1b** or **1c** (1 eq.), 2-pyridinecarboxaldehyde (1.5 eq.) and TFA (0.1 eq.) were dissolved in ethanol (25 ml). Anhydrous $MgSO_4$ (5 eq.) was added and the brown reaction mixture was refluxed for 24 h. Thereafter, the resulting brown mixture was filtered by gravity and the solvent of the filtrate was removed to give a brown residue. To this crude residue, 1 M NaOH (50 ml) was added and the mixture was extracted using DCM (3 × 50 ml). The organic fractions were combined and washed with brine (2 × 50 ml). The organic layer was collected, dried over anhydrous Na_2SO_4, filtered by gravity and the solvent of the filtrate was removed to afford a dull orange/brown solid. The crude product was purified by column chromatography (silica gel) using EtOAc (100%). Compounds **3a** − **3c** were isolated as pale-yellow or beige powders and dried *in vacuo*.

4.2.1. 7-chloro-N-(3-(2-(pyridin-2-yl)-1H-benzo[d]imidazol-1-yl) propyl)quinolin-4-amine (**3a**)

Compound **1a** (0.222 g, 0.680 mmol), 2-pyridinecarboxaldehyde (0.0971 ml, 1.02 mmol), TFA (0.00520 ml, 0.0680 mmol) and anhydrous $MgSO_4$ (0.409 g, 3.40 mmol). Product: Pale-yellow powder. Yield: 0.166 g, 59.1%. M.p. 201.9–203.0 °C. ^{1}H NMR (400 MHz, DMSO-d_6): δ 8.47 (ddd, $^3J_{HH}$ = 4.8, $^4J_{HH}$ = 1.8, $^5J_{HH}$ = 0.9 Hz, 1H, ArH), 8.34 (d, $^3J_{HH}$ = 5.5 Hz, 1H, ArH), 8.27 (dt, $^3J_{HH}$ = 8.0, 1.2 Hz, 1H, ArH), 8.21 (d, $^3J_{HH}$ = 9.1 Hz, 1H, ArH), 7.90 (td, $^3J_{HH}$ = 7.8, $^4J_{HH}$ = 1.8 Hz, 1H, ArH), 7.79 (d, $^4J_{HH}$ = 2.3 Hz, 1H, ArH), 7.76–7.71 (overlapping m, 2H, ArH), 7.44 (dd, $^3J_{HH}$ = 9.1, $^4J_{HH}$ = 2.3 Hz, 1H, ArH), 7.36 (ddd, $^3J_{HH}$ = 7.6, $^3J_{HH}$ = 4.8, $^4J_{HH}$ = 1.2 Hz, 1H, ArH), 7.33–7.25 (overlapping m, 3H, NH/ArH), 6.34 (d, $^3J_{HH}$ = 5.5 Hz, 1H, ArH), 4.99 (t, $^3J_{HH}$ = 7.3 Hz, 2H, CH_2), 3.29 (m, 2H, CH_2), 2.23 (m, 2H, CH_2). ^{13}C{^{1}H} NMR (101 MHz, DMSO-d_6): δ 152.3, 150.4 (2C), 149.9, 149.6, 149.1, 142.6, 137.7, 136.9, 133.8, 128.0, 124.8, 124.5 (3C), 123.6, 122.9, 120.1, 118.0, 111.3, 99.1, 43.3, 40.1, 29.0. IR (ATR, cm^{-1}): ν = 3194 (N–H), 1609 (C=$N_{benz/quin}$), 1592 (C=N_{pyr}), 1580 (C=C). ESI-MS: *m*/*z* 414.1485 (100%, $[M+H]^+$), calculated 414.1480. HPLC purity 99% (t_R = 2.62 min).

4.2.2. 7-chloro-N-(3-(5-methyl-2-(pyridin-2-yl)-1H-benzo[d] imidazol-1-yl)propyl)quinolin-4-amine (**3b**)

Compound **1b** (0.186 g, 0.545 mmol), 2-pyridinecarboxaldehyde (0.0777 ml, 0.817 mmol), TFA (0.00417 ml, 0.0545 mmol) and anhydrous $MgSO_4$ (0.331 g, 2.75 mmol). Product: Beige powder. Yield: 0.146 g, 62.4%. M.p. 216.0–217.5 °C. ^{1}H NMR (300 MHz, DMSO-d_6): δ 8.46 (d, $^3J_{HH}$ = 4.8 Hz, $^4J_{HH}$ = 1.7 Hz, $^5J_{HH}$ = 0.9 Hz 1H, ArH), 8.34 (d, $^3J_{HH}$ = 5.5 Hz, 1H, ArH), 8.25 (dt, $^3J_{HH}$ = 8.0 Hz, $^4J_{HH}$ = 1.0 Hz, 1H, ArH), 8.21 (d, $^3J_{HH}$ = 9.1 Hz, 1H, ArH), 7.89 (td, $^3J_{HH}$ = 7.8, $^4J_{HH}$ = 1.8 Hz, 1H, ArH), 7.79 (d, $^4J_{HH}$ = 2.3 Hz, 1H, ArH), 7.60 (d, $^3J_{HH}$ = 8.3 Hz, 1H, ArH), 7.52 (m, 1H, ArH), 7.44 (dd, $^3J_{HH}$ = 9.1, $^4J_{HH}$ = 2.3 Hz, 1H, ArH), 7.35 (ddd, $^3J_{HH}$ = 7.6, $^3J_{HH}$ = 4.8, $^4J_{HH}$ = 1.2 Hz, 1H, ArH), 7.28 (t, $^3J_{HH}$ = 5.5 Hz, 1H, NH), 7.13 (dd, $^3J_{HH}$ = 8.3, $^4J_{HH}$ = 1.2 Hz, 1H, ArH), 6.33 (d, $^3J_{HH}$ = 5.5 Hz, 1H, ArH), 4.95 (t, $^3J_{HH}$ = 7.1 Hz, 2H, CH_2), 3.28 (m, 2H, CH_2), 2.44 (s, 3H, CH_3), 2.20 (m, 2H, CH_2). ^{13}C{^{1}H} NMR (101 MHz, DMSO-d_6): δ 152.2, 150.4, 149.7, 149.4, 149.1, 142.9, 137.6, 135.0, 133.9, 132.0, 127.9, 125.2, 124.7, 124.5, 124.5 (2C), 124.4, 119.6, 118.0, 110.8, 99.1, 43.3, 40.1, 29.0, 21.6. FT-IR (ATR, cm^{-1}): ν = 3171 (N–H), 1611 (C=$N_{benz/quin}$), 1592 (C=N_{pyr}), 1580 (C=C). ESI-MS: *m*/*z* 428.1644 (100%, $[M+H]^+$), calculated 428.1637. HPLC purity >99% (t_R = 2.33 min).

4.2.3. 7-chloro-N-(3-(2-(pyridin-2-yl)-5-(trifluoromethyl)-1H-benzo[d]imidazol-1-yl)propyl)quinolin-4-amine (**3c**)

Compound **1c** (0.402 g, 1.02 mmol), 2-pyridinecarboxaldehyde (0.145 ml, 1.53 mmol), TFA (0.00781 ml, 0.102 mmol), anhydrous $MgSO_4$ (0.616 g, 5.12 mmol). Product: Beige powder. Yield: 0.298 g, 60.7%. M.p. 200.0–201.0 °C. ^{1}H NMR (400 MHz, DMSO-d_6): δ 8.45 (ddd, $^3J_{HH}$ = 4.8, $^4J_{HH}$ = 1.6, $^5J_{HH}$ = 0.8 Hz, 1H, ArH), 8.31 (d, $^3J_{HH}$ = 5.5 Hz, 1H, ArH), 8.24 (dt, $^3J_{HH}$ = 8.0, $^4J_{HH}$ = 1.2 Hz, 1H, ArH), 8.15 (d, $^3J_{HH}$ = 9.1 Hz, 1H, ArH), 8.08 (m, 1H, ArH), 7.95 (d, $^3J_{HH}$ = 8.7 Hz, 1H, ArH), 7.91 (td, $^3J_{HH}$ = 7.8, $^4J_{HH}$ = 1.6 Hz, 1H, ArH), 7.77 (d, $^4J_{HH}$ = 2.3 Hz, 1H, ArH), 7.60 (dd, $^3J_{HH}$ = 8.7, $^4J_{HH}$ = 1.6 Hz, 1H, ArH), 7.41 (dd, $^3J_{HH}$ = 9.1, $^4J_{HH}$ = 2.3 Hz, 1H, ArH), 7.37 (ddd, $^3J_{HH}$ = 7.6, $^3J_{HH}$ = 4.8, $^4J_{HH}$ = 1.2 Hz, 1H, ArH), 7.25 (t, $^3J_{HH}$ = 5.2 Hz, 1H, NH), 6.33 (d, $^3J_{HH}$ = 5.5 Hz, 1H, ArH), 5.01 (t, $^3J_{HH}$ = 7.2 Hz, 2H, CH_2), 3.28 (m, 2H, CH_2), 2.21 (m, 2H, CH_2). ^{13}C{^{1}H} NMR (101 MHz, DMSO-d_6): δ 152.2 (2C), 150.4, 149.7, 149.4, 149.2, 141.9, 139.1, 137.9, 133.9, 127.9, 126.8, 125.1 (2C), 124.5 (2C), 124.0, 120.1, 118.0, 117.4, 112.6, 99.1, 43.8, 40.1, 28.9. FT-IR (ATR, cm^{-1}): ν = 3179 (N–H), 1613 (C=$N_{benz/quin}$), 1590 (C=N_{pyr}), 1580 (C=C), 1330 (C–F). ESI-MS: *m*/*z* 482.1353 (100%, $[M+H]^+$), calculated 482.1354. HPLC purity 99% (t_R = 2.41 min).

4.3. General method for synthesis of C^N-coordinated Ir(III)-Cp* complexes (**4a** − **4c**)

Sodium acetate (1.5 eq.) was added to a stirring solution of ligand **2a**, **2b** or **2c** (1 eq.) in dry DCM (10 ml) and EtOH (2 ml), and the yellow solution was stirred under N_2 for 1.5 h. A solution of pentamethylcyclopentadienyliridium(III) chloride (0.5 eq.) in DCM (20 ml) was added dropwise over 30 min and the orange solution was stirred for a further 24 h. The resulting cloudy orange reaction mixture was filtered through Celite® and the solvent of the filtrate was removed to afford an orange residue. This crude product was purified by column chromatography (aluminium oxide) using $CHCl_3$:MeOH (97:3) for compounds **4a** or **4b**, and $CHCl_3$ (100%) for compound **4c**. Subsequent precipitation from DCM/pentane afforded the desired product as a dull yellow powder, which was collected by suction filtration and dried *in vacuo*.

4.3.1. Unsubstituted cyclometalated Ir(III)-Cp* complex (**4a**)

Sodium acetate (0.0182 g, 0.222 mmol), compound **2a** (0.0581 g, 0.141 mmol), $[Ir(Cp^*)Cl_2]_2$ (0.0560 g, 0.0703 mmol). Product: Dull yellow powder. Yield: 0.0687 g, 63.0%. M.p. 204.0–206.3 °C. ^{1}H NMR (300 MHz, DMSO-d_6): δ 8.40 (d, $^3J_{HH}$ = 9.1 Hz, 1H, ArH), 8.35 (d, $^3J_{HH}$ = 5.4 Hz, 1H, ArH), 8.00 (m, 2H, ArH), 7.83 (d, $^3J_{HH}$ = 7.5 Hz, 1H, ArH), 7.80 (d, $^4J_{HH}$ = 2.2 Hz, 1H, ArH), 7.70 (t, $^3J_{HH}$ = 5.1 Hz, 1H, NH), 7.59–7.47 (overlapping m, 3H, ArH), 7.45 (dd, $^3J_{HH}$ = 9.0, $^4J_{HH}$ = 2.2 Hz, 1H, ArH), 7.27 (t, $^3J_{HH}$ = 7.5 Hz, 1H, ArH), 6.98 (t, $^3J_{HH}$ = 7.5 Hz, 1H, ArH), 6.42 (d, $^3J_{HH}$ = 5.4 Hz, 1H, ArH), 4.99 (m, 2H, CH_2), 3.49 (m, 2H, CH_2), 2.31 (m, 2H, CH_2), 1.72 (s, 15H, Cp*). ^{13}C{^{1}H} NMR (151 MHz, DMSO-d_6): δ 161.7, 154.5, 152.3, 150.4, 149.6, 138.3, 137.5, 136.0, 134.3, 133.9, 131.5, 127.9, 126.4, 125.0, 124.9 (2C), 124.9, 124.6, 118.1, 116.0, 113.0, 99.1, 96.3 (5C), 43.2, 40.5, 28.3, 9.2 (5C). FT-IR (ATR, cm^{-1}): ν = 3254 (N–H), 1609 (C=N_{quin}), 1580 (C=C/C=N_{benz}). ESI-MS: *m*/*z* 370.1120 (100%, $[M-Cl+H]^{2+}$), calculated 370.1129; *m*/*z* 773.1756 (60%, $[M-H]^-$), calculated 773.1795.

4.3.2. Methyl-substituted cyclometalated Ir(III)-Cp complex (**4b**)*

Sodium acetate (0.0182 g, 0.222 mmol), compound **2b** (0.0599 g, 0.140 mmol), $[Ir(Cp^*)Cl_2]_2$ (0.0559 g, 0.0702 mmol). Product: Dull yellow powder. Yield: 0.0689 g, 62.6%. M.p. 204.4–207.2 °C. ^{1}H NMR (400 MHz, DMSO-d_6): δ 8.38–8.35 (overlapping m, 2H, ArH), 7.93 (d, $^3J_{HH}$ = 7.8 Hz, 1H, ArH), 7.89 (d, $^3J_{HH}$ = 8.5 Hz, 1H, ArH), 7.80 (m, 2H, ArH), 7.72 (t, $^3J_{HH}$ = 4.4 Hz, 1H, NH), 7.47 (dd, $^3J_{HH}$ = 9.0, $^4J_{HH}$ = 2.2 Hz, 1H, ArH), 7.33 (d, $^3J_{HH}$ = 8.5 Hz, 1H, ArH), 7.27–7.23 (overlapping m, 2H, ArH), 6.90 (t, $^3J_{HH}$ = 7.3 Hz, 1H, ArH), 6.44 (d, $^3J_{HH}$ = 5.5 Hz, 1H, ArH), 4.94 (m, 2H, CH_2), 3.47 (m, 2H, CH_2), 2.56 (s, 3H, CH_3), 2.25 (m, 2H, CH_2), 1.72 (s, 15H, Cp*). $^{13}C\{^1H\}$ NMR (101 MHz, DMSO-d_6): δ 161.4, 154.2, 152.3, 150.4, 149.6, 138.6, 137.4, 134.7, 134.3, 134.2, 133.9, 131.4, 127.9, 126.3, 126.2, 124.9, 124.7, 124.6, 118.0, 115.4, 112.7, 99.1, 96.3 (5C), 43.1, 40.3, 28.4, 21.7, 9.2 (5C). FT-IR (ATR, cm^{-1}): ν = 3274 (N–H), 1611 (C=N_{quin}), 1584 (C=C/C=N_{benz}). ESI-MS: *m/z* 370.1207 (100%, $[M-Cl+H]^{2+}$), calculated 377.1207; *m/z* 787.1949 (50%, $[M-H]^-$), calculated 787.1952.

4.3.3. Trifluoromethyl-substituted cyclometalated Ir(III)-Cp complex (**4c**)*

Sodium acetate (0.0259 g, 0.316 mmol), compound **4c** (0.0754 g, 0.157 mmol), $[Ir(Cp^*)Cl_2]_2$ (0.0624 g, 0.0784 mmol). Product: Yellow powder. Yield: 0.0683 g, 51.7%. M.p. 201.1–203.1 °C.^{1}H NMR (600 MHz, DMSO-d_6): δ 8.38 (d, $^3J_{HH}$ = 9.0 Hz, 1H, ArH), 8.35 (d, $^3J_{HH}$ = 5.5 Hz, 1H, ArH), 8.32 (d, $^3J_{HH}$ = 8.6 Hz, 1H, ArH), 7.99 (d, $^3J_{HH}$ = 7.8 Hz, 1H, ArH), 7.85–7.82 (overlapping m, 2H, ArH), 7.79 (d, $^4J_{HH}$ = 2.3 Hz, 1H, ArH), 7.75 (t, $^3J_{HH}$ = 5.5 Hz, 1H, NH), 7.69 (m, 1H, ArH), 7.45 (dd, $^3J_{HH}$ = 9.0, $^4J_{HH}$ = 2.3 Hz, 1H, ArH), 7.29 (td, $^3J_{HH}$ = 7.8, $^4J_{HH}$ = 1.1 Hz, 1H, ArH), 6.89 (td, $^3J_{HH}$ = 7.8, $^4J_{HH}$ = 1.1 Hz, 1H, ArH), 6.47 (d, $^3J_{HH}$ = 5.5 Hz, 1H, ArH), 5.02 (m, 2H, CH_2), 3.52 (m, 2H, CH_2), 2.29 (m, 2H, CH_2), 1.70 (s, 15H, Cp*). $^{13}C\{^1H\}$ NMR (151 MHz, DMSO-d_6): δ 164.3, 155.6, 152.3, 150.4, 149.6, 138.7, 138.2, 137.3, 133.9, 133.6, 132.3, 127.9, 127.52, 127.1, 125.3, 125.0, 124.8, 124.6, 121.4, 118.0, 114.6, 112.8, 99.2, 96.4 (5C), 43.8, 40.5, 28.2, 9.2 (5C). FT-IR (ATR, cm^{-1}): ν = 3274 (N–H), 1611 (C=N_{quin}), 1584 (C=C/C=N_{benz}), 1326 (C–F). ESI-MS: *m/z* 404.1064 (100%, $[M-Cl+H]^{2+}$), calculated 404.1066; *m/z* 807.2033 (70%, $[M-Cl]^-$), calculated 807.2053; *m/z* 841.1702 (100%, $[M-H]^-$), calculated 841.1669.

4.4. General method for synthesis of C^N-coordinated Rh(III)-Cp complexes (**5a** – **5b**)*

Sodium acetate (2 eq.) was added to a stirring solution of ligand **2a** or **2b** (1 eq.) in dry methanol (15 ml) and the pale-yellow solution was stirred under N_2 for 30 min. Thereafter, a solution of pentamethylcyclopentadienylrhodium(III) chloride dimer (0.5 eq.) in dry DCM (20 ml) was added dropwise over 10 min and the red solution was refluxed under N_2 for 96 h. The resulting red solution was cooled to room temperature and the solvent was removed to afford a red residue. This crude residue was purified by column chromatography (aluminium oxide) using $CHCl_3$:MeOH (19:1). Precipitation from DCM/pentane afforded the desired product as a dull orange powder, which was collected by suction filtration and dried *in vacuo*.

4.4.1. Unsubstituted cyclometalated Rh(III)-Cp complex (**5a**)*

Sodium acetate (0.0217 g, 0.264 mmol), compound **2a** (0.0514 g, 0.124 mmol), $[Rh(Cp^*)Cl_2]_2$ (0.0382 g, 0.0618 mmol). Product: Dull orange powder. Yield: 0.0304 g, 35.9%. M.p. 186.8 °C (Decomp. w/o melting). ^{1}H NMR (300 MHz, DMSO-d_6): δ 8.39–8.32 (overlapping m, 2H, ArH), 8.01 (dd, $^3J_{HH}$ = 6.9, $^4J_{HH}$ = 1.9 Hz, 1H, ArH), 7.93 (d, $^3J_{HH}$ = 7.5 Hz, 1H, ArH), 7.83–7.79 (overlapping m, 2H, ArH), 7.66–7.59 (overlapping m, 2H, NH/ArH), 7.54–7.43 (overlapping m, 3H, ArH), 7.32 (t, $^3J_{HH}$ = 7.4 Hz, 1H, ArH), 6.90 (t, $^3J_{HH}$ = 7.2 Hz, 1H, ArH), 6.45 (d, $^3J_{HH}$ = 5.5 Hz, 1H, ArH), 4.92 (m, 2H, CH_2), 3.47 (m, 2H, CH_2), 2.26 (m, 2H, CH_2), 1.64 (s, 15H, Cp*). $^{13}C\{^1H\}$ NMR (151 MHz, DMSO-d_6): δ 158.4, 152.7, 151.1, 149.5, 139.2, 138.2, 136.8, 135.1, 134.8, 131.7, 128.0, 126.7, 126.0, 125.4, 125.3 (2C), 124.9 (2C), 118.3, 116.8, 113.2, 102.5 (d, $^1J_{RhC}$ = 4.6 Hz, 5C), 99.7, 43.7, 40.5, 28.6, 9.9 (5C). FT-IR (ATR, cm^{-1}): ν = 3266 (N–H), 1611 (C=N_{quin}), 1580 (C=C/C=N_{benz}). ESI-MS: *m/z* 325.0846 (100%, $[M-Cl+H]^{2+}$), calculated 325.0842; *m/z* 649.1589 (30%, $[M-Cl]^+$), calculated 649.1605.

4.4.2. Methyl-substituted cyclometalated Rh(III)-Cp complex (**5b**)*

Sodium acetate (0.0320 g, 0.390 mmol), compound **2b** (0.0801 g, 0.188 mmol), $[Rh(Cp^*)Cl_2]_2$ (0.0580 g, 0.0938 mmol). Product: Dull orange powder. Yield: 0.0613 g, 46.8%. M.p. 194.2 °C (Decomp. w/o melting). ^{1}H NMR (600 MHz, DMSO-d_6): δ 8.39 (d, $^3J_{HH}$ = 9.1 Hz, 1H, ArH), 8.34 (d, $^3J_{HH}$ = 5.4 Hz, 1H, ArH), 7.92–7.87 (overlapping m, 2H, ArH), 7.82–7.77 (overlapping m, 2H, ArH), 7.68 (t, $^3J_{HH}$ = 5.4 Hz, 1H, NH), 7.47 (dd, $^3J_{HH}$ = 9.0, $^4J_{HH}$ = 2.3 Hz, 1H, ArH), 7.34 (m, 1H, ArH), 7.33–7.26 (m, 2H, ArH), 6.89 (td, $^3J_{HH}$ = 7.8, $^4J_{HH}$ = 1.0 Hz, 1H, ArH), 6.43 (d, $^3J_{HH}$ = 5.5 Hz, 1H, ArH), 4.88 (m, 2H, CH_2), 3.46 (m, 2H, CH_2), 2.54 (s, 3H, CH_3), 2.23 (m, 2H, CH_2), 1.63 (s, 15H, Cp*). $^{13}C\{^1H\}$ NMR (151 MHz, DMSO-d_6): δ 157.7, 152.3, 150.4, 149.6, 139.2, 137.6, 134.7, 134.6, 134.4, 133.9, 131.0, 127.9, 126.2, 126.1, 125.4, 124.8 (2C), 124.6, 118.0, 115.8, 112.6, 101.9 (d, $^1J_{RhC}$ = 4.7 Hz, 5C), 99.1, 43.3, 40.5, 28.3, 21.6, 9.5 (5C). FT-IR (ATR, cm^{-1}): ν = 3258 (N–H), 1611 (C=N_{quin}), 1580 (C=C/C=N_{benz}). ESI-MS: *m/z* 332.0920 (100%, $[M-Cl+H]^{2+}$), calculated 332.0920; *m/z* 663.1749 (28%, $[M-Cl]^+$), calculated 663.1761.

4.5. General method for synthesis of N^N-coordinated Ir(III)- and Rh(III)-Cp complexes (**6a** – **6c** and **7a** – **7c**)*

Pentamethylcyclopentadienyliridium(III) chloride dimer (0.5 eq.) or pentamethyl-cyclopentadienylrhodium(III) chloride dimer (0.5 eq.) dissolved in DCM (10 ml) was added dropwise to a stirring solution of ligand **3a**, **3b** or **3c** (1 eq.) in EtOH (10 ml) and the orange solution was stirred at room temperature under N_2 for 16–24 h. The DCM was then removed, NH_4PF_6 (1.2 eq.) was added and the solution was stirred at 0 °C for 2 h, resulting in the precipitation of the product as a yellow or orange solid. Thereafter, the solvent was reduced and the mixture placed in the fridge overnight. The resulting precipitate was collected by suction filtration and washed with cold ethanol, followed by diethyl ether and dried *in vacuo*.

4.5.1. Unsubstituted N^N-coordinated Ir(III)-Cp complex (**6a**)*

$[Ir(Cp^*)Cl_2]_2$ (0.0494 g, 0.0620 mmol), compound **3a** (0.0512 g, 0.124 mmol) and NH_4PF_6 (0.0255 g, 0.156 mmol). Product: Yellow powder. Yield: 0.0759 g, 66.4%. M.p. 189.3–192.3 °C. ^{1}H NMR (400 MHz, DMSO-d_6): δ 9.12 (dd, $^3J_{HH}$ = 5.6 Hz, $^4J_{HH}$ = 1.0 Hz, 1H, ArH), 8.56 (d, $^3J_{HH}$ = 8.2 Hz, 1H, ArH), 8.40 (d, $^3J_{HH}$ = 5.7 Hz, 1H, ArH), 8.26 (d, $^3J_{HH}$ = 9.1 Hz, 1H, ArH), 8.11–8.06 (overlapping m, 2H, NH/ArH), 7.86–7.82 (overlapping m, 2H, ArH), 7.76 (m, 1H, ArH), 7.66–7.58 (overlapping m, 3H, ArH), 7.53 (dd, $^3J_{HH}$ = 9.1, $^4J_{HH}$ = 2.2 Hz, 1H, ArH), 6.50 (d, $^3J_{HH}$ = 5.7 Hz, 1H, ArH), 5.08 (m, 2H, CH_2), 3.50 (m, 2H, CH_2), 2.31 (m, 2H, CH_2), 1.69 (s, 15H, Cp*). $^{13}C\{^1H\}$ NMR (101 MHz, DMSO-d_6): δ 154.3, 151.2, 151.0, 150.9, 148.0, 145.6, 140.8, 137.7, 136.4, 134.6, 129.1, 126.9, 126.7, 126.0, 125.1, 125.0, 124.6, 117.8, 117.6, 113.4, 99.2, 89.1 (5C), 43.7, 40.5, 28.4, 9.3 (5C). $^{31}P\{^1H\}$ NMR (162 MHz, DMSO-d_6): δ −144.2 (sep, ^1J = 711.2 Hz, PF_6^-). FT-IR (ATR, cm^{-1}): ν = 3333 (N–H), 1633 (sh, C=N_{pyr}), 1609 (C=$N_{benz/quin}$), 1580 (C=C). ESI-MS: *m/z* 388.5986 ($[M+H]^{2+}$), calculated 388.5986.

4.5.2. Methyl-substituted N^N-coordinated Ir(III)-Cp complex (**6b**)*

$[Ir(Cp^*)Cl_2]_2$ (0.0485 g, 0.0609 mmol), compound **3b** (0.0521 g, 0.122 mmol) and NH_4PF_6 (0.0255 g, 0.156 mmol). Product: Yellow powder. Yield: 0.0805 g, 70.7%. M.p. 200.8–202.5 °C. ^{1}H NMR (600 MHz, DMSO-d_6): δ 9.10 (dd, $^3J_{HH}$ = 5.6, $^4J_{HH}$ = 1.3 Hz, 1H, ArH), 8.54

(d, $^3J_{HH}$ = 8.2 Hz, 1H, ArH), 8.43 (d, $^3J_{HH}$ = 6.0 Hz, 1H, ArH), 8.26 (d, $^3J_{HH}$ = 9.1 Hz, 1H, ArH), 8.11 (td, $^3J_{HH}$ = 8.2, $^4J_{HH}$ = 1.3 Hz, 1H, ArH), 7.99 (m, 1H, NH), 7.95 (d, $^3J_{HH}$ = 8.6 Hz, 1H, ArH), 7.85–7.81 (overlapping m, 2H, ArH), 7.57 (dd, $^3J_{HH}$ = 9.1, $^4J_{HH}$ = 2.2 Hz, 1H, ArH), 7.45 (m, 1H, ArH), 7.43 (dd, $^3J_{HH}$ = 8.6, $^4J_{HH}$ = 1.1 Hz, 1H, ArH), 6.57 (d, $^3J_{HH}$ = 6.0 Hz, 1H, ArH), 5.04 (m, 2H, CH_2), 3.52 (m, 2H, CH_2), 2.56 (s, 3H, CH_3), 2.29 (m, 2H, CH_2), 1.68 (s, 15H, Cp*). $^{13}C\{^1H\}$ NMR (151 MHz, DMSO-d_6): δ 154.3, 152.1, 150.7, 149.6, 146.0, 145.7, 140.9, 138.0, 135.9, 135.5, 134.7, 129.1, 128.4, 125.6, 125.3, 124.9, 124.8, 117.3, 116.9, 113.2, 99.2, 89.1 (5C), 43.7, 40.5, 28.4, 21.6, 9.4 (5C). $^{31}P\{^1H\}$ NMR (162 MHz, DMSO-d_6): δ −144.2 (sep, ^1J = 711.2 Hz, PF_6^-). FT-IR (ATR, cm^{-1}): ν = 3337 (N—H), 1633 (sh, C=N_{pyr}), 1613 (C=$N_{benz/quin}$), 1580 (C=C). ESI-MS: *m/z* 395.6066 ($[M+H]^{2+}$), calculated 395.6064.

4.5.3. Trifluoromethyl-substituted N^gN-coordinated Ir(III)-Cp* complex (**6c**)

$[Ir(Cp^*)Cl_2]_2$ (0.0436 g, 0.0547 mmol), compound **3c** (0.0526 g, 0.109 mmol) and NH_4PF_6 (0.0236 g, 0.145 mmol). Product: Yellow powder. Yield: 0.0573 g, 53.0%. M.p. 244.5–247.2 °C. ^1H NMR (400 MHz, DMSO-d_6): δ 9.16 (dd, $^3J_{HH}$ = 5.6, $^4J_{HH}$ = 1.1 Hz, 1H, ArH), 8.63 (d, $^3J_{HH}$ = 8.2 Hz, 1H, ArH), 8.41 (d, $^3J_{HH}$ = 5.6 Hz, 1H, ArH), 8.35 (d, $^3J_{HH}$ = 9.2 Hz, 1H, ArH), 8.18–8.09 (overlapping m, 2H, ArH), 7.97–7.87 (overlapping m, 3H, ArH), 7.81 (d, $^4J_{HH}$ = 2.2 Hz, 1H, ArH), 7.60 (t, $^3J_{HH}$ = 5.5 Hz, 1H, NH), 7.49 (dd, $^3J_{HH}$ = 9.0, $^4J_{HH}$ = 2.2 Hz, 1H, ArH), 6.52 (d, $^3J_{HH}$ = 5.7 Hz, 1H, ArH), 5.14 (m, 2H, CH_2), 3.53 (m, 2H, CH_2), 2.36 (m, 2H, CH_2), 1.69 (s, 15H, Cp*). $^{13}C\{^1H\}$ NMR (151 MHz, DMSO-d_6): δ 154.4, 153.7, 151.1, 151.0, 147.8, 145.1, 141.0, 138.9, 137.1, 134.6, 129.9, 126.1, 125.9, 125.8, 125.4, 125.1, 124.6, 123.0, 117.6, 115.5, 114.5, 99.3, 89.3 (5C), 44.4, 40.5, 28.2, 9.4 (5C). $^{31}P\{^1H\}$ NMR (162 MHz, DMSO-d_6): δ −144.2 (sep, ^1J = 711.2 Hz, PF_6^-). FT-IR (ATR, cm^{-1}): ν = 3337 (N—H), 1633 (sh, C=N_{pyr}), 1611 (sh, C=$N_{benz/quin}$), 1582 (C=C), 1330 (C—F). ESI-MS: *m/z* 422.5920 ($[M+H]^{2+}$), calculated 422.5923.

4.5.4. Unsubstituted N^N-coordinated Rh(III)-Cp* complex (**7a**)

$[Rh(Cp^*)Cl_2]_2$ (0.0382 g, 0.0618 mmol), compound **3a** (0.0512 g, 0.124 mmol) and NH_4PF_6 (0.0243 g, 0.149 mmol). Product: Orange powder. Yield: 0.0723 g, 70.2%. M.p. 194.9–197.0 °C. ^1H NMR (400 MHz, DMSO-d_6): δ 9.12 (dd, $^3J_{HH}$ = 5.4, $^4J_{HH}$ = 0.9 Hz, 1H, ArH), 8.48 (d, $^3J_{HH}$ = 8.2 Hz, 1H, ArH), 8.41 (d, $^3J_{HH}$ = 5.8 Hz, 1H, ArH), 8.25 (d, $^3J_{HH}$ = 9.1 Hz, 1H, ArH), 8.11–8.04 (overlapping m, 2H, ArH), 7.87 (m, 1H, ArH), 7.85–7.80 (overlapping m, 2H, ArH), 7.73 (t, $^3J_{HH}$ = 5.5 Hz, 1H, NH), 7.62–7.57 (overlapping m, 2H, ArH), 7.54 (dd, $^3J_{HH}$ = 9.1, $^4J_{HH}$ = 2.2 Hz, 1H, ArH), 6.53 (d, $^3J_{HH}$ = 5.8 Hz, 1H, ArH), 5.01 (m, 2H, CH_2), 3.55 (m, 2H, CH_2), 2.29 (m, 2H, CH_2), 1.68 (s, 15H, Cp*). $^{13}C\{^1H\}$ NMR (101 MHz, DMSO-d_6): δ 154.3, 151.4, 150.8, 148.3, 147.5, 145.7, 140.8, 138.5, 137.0, 134.9, 128.5, 126.5, 126.4, 125.7, 125.3, 124.9, 124.7, 118.3, 117.5, 113.3, 99.3, 97.1 (d, $^1J_{RhC}$ = 7.8 Hz, 5C), 43.8, 40.5, 28.3, 9.5 (5C). $^{31}P\{^1H\}$ NMR (162 MHz, DMSO-d_6): δ −144.2 (sep, ^1J = 711.2 Hz, PF_6^-). FT-IR (ATR, cm^{-1}): ν = 3329 (N—H), 1633 (sh, C=N_{pyr}), 1609 (C=$N_{benz/quin}$), 1580 (C=C). ESI-MS: *m/z* 325.5818 ($[M - Cl]^{2+}$), calculated 325.5818.

4.5.5. Methyl-substituted N^N-coordinated Rh(III)-Cp* complex (**7b**)

$[Rh(Cp^*)Cl_2]_2$ (0.0372 g, 0.0602 mmol), compound **3b** (0.0515 g, 0.120 mmol) and NH_4PF_6 (0.0253 g, 0.155 mmol). Product: Orange powder. Yield: 0.0842 g, 82.7%. M.p. 201.1–202.6 °C. ^1H NMR (600 MHz, DMSO-d_6): δ 9.10 (dd, $^3J_{HH}$ = 5.5, $^4J_{HH}$ = 1.1 Hz, 1H, ArH), 8.45 (d, $^3J_{HH}$ = 7.9 Hz, 1H, ArH), 8.44 (d, $^3J_{HH}$ = 6.1 Hz, 1H, ArH), 8.24 (d, $^3J_{HH}$ = 9.1 Hz, 1H, ArH), 8.11 (td, $^3J_{HH}$ = 7.9, $^4J_{HH}$ = 1.1 Hz, 1H, ArH), 8.01 (m, 1H, NH), 7.93 (d, $^3J_{HH}$ = 8.6 Hz, 1H, ArH), 7.86 (ddd, $^3J_{HH}$ = 7.9, $^3J_{HH}$ = 5.5, $^4J_{HH}$ = 1.0 Hz, 1H, ArH), 7.84 (d, $^4J_{HH}$ = 2.2 Hz, 1H, ArH), 7.58 (dd, $^3J_{HH}$ = 9.0, $^4J_{HH}$ = 2.2 Hz, 1H, ArH), 7.51 (dt, $^3J_{HH}$ = 1.5, $^4J_{HH}$ = 0.9 Hz, 1H, ArH), 7.39 (dd, $^3J_{HH}$ = 8.6, $^4J_{HH}$ = 1.5 Hz, 1H, ArH), 6.58 (d, $^3J_{HH}$ = 6.1 Hz, 1H, ArH), 4.97 (m, 2H, CH_2), 3.52 (m, 2H, CH_2), 2.55 (s, 3H, CH_3), 2.26 (m, 2H, CH_2), 1.67 (s, 15H, Cp*). $^{13}C\{^1H\}$ NMR (151 MHz, DMSO-d_6): δ 154.3, 152.3, 149.3, 148.0, 145.8 (2C), 140.8, 138.8, 135.6, 135.4, 135.2, 128.4, 128.1, 125.7, 125.1, 124.9, 124.8, 117.4, 117.2, 113.0, 99.2, 97.0 (d, $^1J_{RhC}$ = 7.8 Hz, 5C), 43.8, 40.5, 28.3, 21.6, 9.6 (5C). $^{31}P\{^1H\}$ NMR (162 MHz, DMSO-d_6): δ −144.2 (sep, ^1J = 711.2 Hz, PF_6^-). FT-IR (ATR, cm^{-1}): ν = 3329 (N—H), 1633 (sh, C=N_{pyr}), 1613 (C=$N_{benz/quin}$), 1582 (C=C). ESI-MS: *m/z* 332.5899 ($[M - Cl]^{2+}$), calculated 332.5896.

4.5.6. Trifluoromethyl-substituted N^N-coordinated Rh(III)-Cp* complex (**7c**)

$[Rh(Cp^*)Cl_2]_2$ (0.0335 g, 0.0542 mmol), compound **3c** (0.0521 g, 0.108 mmol) and NH_4PF_6 (0.0211 g, 0.129 mmol). Product: Orange powder. Yield: 0.0805 g, 82.7%. M.p. 202.0–204.7 °C. ^1H NMR (400 MHz, DMSO-d_6): δ 9.17 (d, $^3J_{HH}$ = 5.2 Hz, 1H, ArH), 8.56 (d, $^3J_{HH}$ = 7.9 Hz, 1H, ArH), 8.46 (d, $^3J_{HH}$ = 6.1 Hz, 1H, ArH), 8.30 (d, $^3J_{HH}$ = 8.8 Hz, 1H, ArH), 8.21 (t, $^3J_{HH}$ = 7.9 Hz, 1H, ArH), 8.11 (d, $^3J_{HH}$ = 9.1 Hz, 1H, ArH), 8.04 (m, 1H, NH), 8.00–7.92 (overlapping m, 2H, ArH), 7.87–7.82 (overlapping m, 2H, ArH), 7.57 (dd, $^3J_{HH}$ = 9.1, $^4J_{HH}$ = 1.5 Hz, 1H, ArH), 6.62 (d, $^3J_{HH}$ = 6.1 Hz, 1H, ArH), 5.08 (m, 2H, CH_2), 3.58 (m, 2H, CH_2), 2.35 (m, 2H, CH_2), 1.68 (s, 15H, Cp*). $^{13}C\{^1H\}$ NMR (101 MHz, DMSO-d_6): δ 154.4, 152.6, 151.0, 148.7, 145.2, 141.0, 139.4, 137.8, 135.9, 129.2, 126.1, 125.9, 125.7, 125.1, 124.9, 124.4, 122.6, 116.9, 115.3, 115.0, 114.9, 99.2, 97.3 (d, $^1J_{RhC}$ = 7.8 Hz, 5C), 44.5, 40.4, 28.0, 9.5 (5C). $^{31}P\{^1H\}$ NMR (162 MHz, DMSO-d_6): δ −144.2 (sep, ^1J = 711.2 Hz, PF_6^-). FT-IR (ATR, cm^{-1}): ν = 3341 (N—H), 1631 (sh, C=N_{pyr}), 1613 (C=$N_{benz/quin}$), 1582 (C=C), 1330 (C—F). ESI-MS: *m/z* 240.0528 ($[M-Cl + H]^{3+}$), calculated 240.0529.

4.6. X-ray structure determination

Single-crystal X-ray diffraction data were collected on a Bruker KAPPA APEX II DUO diffractometer using graphite-monochromated Mo-Kα radiation (χ = 0.71073 Å). Data collection was carried out at 100(2) K. Temperature was controlled by an Oxford Cryostream cooling system (Oxford Cryostat). Cell refinement and data reduction were performed using the program SAINT [40]. The data were scaled, and absorption correction performed using SADABS [41]. The structures were solved by direct methods using SHELXS-97 [41] and refined by full-matrix least-squares methods based on F^2 using SHELXL-2018 [41] and using the graphics interface program X-Seed [42,43]. The programs X-Seed and POV-Ray [44] were used to prepare molecular graphic images.

There are two molecules of compound **6b** and three and half acetone solvent molecules in the asymmetric unit. The half acetone molecule was disordered and located on the centre of conversion. All non-hydrogen atoms, except the disordered acetone, were refined anisotropically. All hydrogen atoms were placed in idealised positions and refined in riding models with U_{iso} assigned 1.2 or 1.5 times U_{eq} of their parent atoms and the bond distances were constrained to 0.88 Å for N—H, 0.95 Å, 0.98 Å and 0.99 Å for different types of *C*—H. The structure was refined to R factor of 0.0400.

4.7. Plasmodium falciparum assay

The samples were tested against the chloroquine-sensitive NF54 strain and chloroquine-resistant K1 strain of *P. falciparum*. Continuous *in vitro* cultures of asexual erythrocyte stages of *P. falciparum* were maintained using a modified method of Trager and Jensen [45]. The *in vitro* antiplasmodium activity was determined *via* the parasite lactate dehydrogenase (pLDH) assay using a modified method described by Makler et al. [29] The samples were prepared as 20 mg/ml stock solutions using dimethyl sulfoxide (DMSO) and

sonicated to enhance solubility. Samples were tested as a suspension if not completely dissolved. Stock solutions were stored at −20 °C and further dilutions were prepared on the day of the experiment. Chloroquine was used as the reference drug in all experiments. A full dose-response measurement was performed for all compounds to determine the concentration inhibiting 50% of parasite growth (IC_{50} value). The samples were tested at a starting concentration of 10 μg/ml, which was then serially diluted 2-fold in complete medium to give 10 concentrations; with the lowest concentration being 0.02 μg/ml. The same dilution technique was used for all samples. The positive control drugs were tested at a starting concentration of 10 μg/ml. The highest concentration of solvent to which the parasites were exposed had no measurable effect on the parasite viability. The IC_{50} values were obtained using a non-linear dose-response curve fitting analysis *via* Graph Pad Prism v.5.0 software.

4.8. In vitro cytotoxicity assay

In vitro cytotoxicity of potent target compounds against the Chinese Hamster Ovarian (CHO) cells was determined using the 3-(4,5-dimethylthiazol-2-yl)-2,5-diphenyltetrazolium bromide (MTT) assay, which determines cellular growth and survival [30,31]. For each test compound, a stock solution (2 mg/mL) was prepared in 10% DMSO, and then diluted with the assay medium to yield a starting concentration of a 100 μg/mL. This was then serially diluted (10-fold) to give six assay concentrations ranging from 100 to 0.001 μg/mL. The positive control drug, emetine, was subjected to similar dilutions. In all cases, samples were tested in triplicate. The highest concentration of DMSO used had no measurable effect on cell viability. A solution of MTT was then added after 44 h of exposure of the cells to the test compound, followed by a further 4 h of incubation at 37 °C. The supernatant was then separated from the cells by suction and the formazan crystals were dissolved by addition of DMSO to each well. The amount of formazan in each well was determined by measuring the absorbance at 540 nm. The IC_{50} values were obtained from dose-response curves, using a non-linear dose-response curve analysis *via* GraphPad Prism v.5.0 software.

4.9. β-Haematin inhibition assay

The β-haematin formation assay was adapted from the method described by Sandlin et al. [32]. Test compounds were prepared as a 10 mM stock solution in 100% DMSO. Compounds were tested at concentrations between 500 μM and 5 μM. The stock solution was serially diluted to give 12 concentrations in a 96 well flat-bottom assay plate. NP-40 detergent was then added to mediate the formation of β-haematin (30.55 μM, final concentration). A 25 mM stock solution of haematin was prepared by dissolving haemin (16.3 mg) in DMSO (1 ml). A 177.76 μl aliquot of haematin stock was suspended in 20 ml of a 2 M acetate buffer (pH 4.7). The haematin suspension was then added to the plate to give a final haematin concentration of 100 μM. The plate was then incubated for 16 h at 37 °C. The assay was analysed using the pyridine ferrihaemochrome method developed by Ncokazi and Egan [33]. Thirty-two microlitres of a solution of 50% pyridine, 20% acetone, 20% water, and 10% 2 M HEPES buffer (pH 7.4) was added to each well. To this, 60 μl of acetone was then added to each well and mixed. The absorbance of the resulting complex was measured at 405 nm on a SpectraMax 340 PC plate reader. The IC_{50} values were obtained using a non-linear dose-response curve fitting analysis *via* Graph Pad Prism v.5.0 software.

4.10. Antimycobacterial MIC assay

The minimum inhibitory concentration (MIC) values were determined using the standard broth microdilution method [46], where a 10 ml culture of *Mycobacterium tuberculosis* H37Rv [47], was grown to an absorbance (OD600) of 0.6–0.7. The media used were Middlebrook 7H9 media (Difco) supplemented with 0.2% Glucose, Middlebrook albumin-dextrose-catalase (ADC) enrichment (Difco) and 0.05% Tween [48], or Middlebrook 7H9 supplemented with 0.03% casitone, 0.4% glucose, and 0.05% tyloxapol [49]. Cultures grown in these media were diluted 1:500 prior to inoculation of the MIC assay. The compounds to be tested were reconstituted to a concentration of 10 mM in DMSO. Duplicate 2-fold serial dilutions of the test compounds were prepared across a 96-well micro titre plate, in a volume of 50 μl, after which 50 μl of the diluted *M. tuberculosis* cultures was added to each well in the plate (including control wells). The final volume per well was 100 μl. The plate layout was a modification of the method previously described [50]. Assay controls used were a minimum growth control (rifampicin at 2 × MIC), and a maximum growth control (5% DMSO). The microtitre plates were sealed in a secondary container and incubated at 37 °C with 5% CO_2 and humidification. Alamar Blue reagent was added to each well of the assay plate 24 h prior to fluorescence reading. Relative fluorescence (excitation 485 nM; emission 520 nM) was measured using a plate reader (FLUOstar OPTIMA, BMG LABTECH) at day 7. The raw fluorescence data was archived and analysed using the CDD Vault from Collaborative Drug Discovery, in which data was normalised to the minimum and maximum inhibition controls to generate a dose response curve (percentage inhibition), using the Levenberg-Marquardt damped least squares method, from which the MIC_{90} was calculated [51]. The lowest concentration of drug that inhibited growth of more than 90% of the mycobacterial population was considered the MIC_{90}.

Declaration of competing interest

The authors declare that they have no known competing financial interests or personal relationships that could have appeared to influence the work reported in this paper.

Acknowledgements

Financial support from the University of Cape Town and the National Research Foundation (NRF; UID: 111707) of South Africa is gratefully acknowledged (G.S.S.). The University of Cape Town, South African Medical Research Council, and South African Research Chairs Initiative of the Department of Science and Technology administered through the South African National Research Foundation are gratefully acknowledged for support (K.C.). All antimycobacterial screening work was conducted in the MMRU (UCT) with the support of the SAMRC through the Strategic Health Innovation Partnerships (SHIP) initiative (to D.F.W.).

Appendix A. Supplementary data

Supplementary data to this article can be found online at https://doi.org/10.1016/j.ejmech.2020.112694.

References

[1] World Health Organisation, World Malaria Report 2019, WHO Press, Geneva, 2019. World Malaria Report.
[2] World Health Organization, Guidelines for the Treatment of Malaria, WHO Press, Geneva, 2015.
[3] M. Enserink, Malaria's Drug Miracle in Danger, American Association for the

Advancement of Science, 2010.
[4] World Health Organization, Global Plan for Artemisinin Resistance Containment (GPARC), WHO Press, Geneva, 2011.
[5] World Health Organisation, Global Tuberculosis Report 2019, WHO Press, Geneva, 2019.
[6] World Health Organization, Treatment of Tuberculosis: Guidelines, WHO Press, Geneva, 2010.
[7] A.A. Velayati, M.R. Masjedi, P. Farnia, P. Tabarsi, J. Ghanavi, A.H. Zia Zarifi, S.E. Hoffner, Emergence of new forms of totally drug-resistant tuberculosis bacilli: super extensively drug-resistant tuberculosis or totally drug-resistant strains in Iran, Chest 136 (2009) 420–425.
[8] B. Meunier, Hybrid molecules with a dual mode of action: dream or reality? Acc. Chem. Res. 41 (2007) 69–77.
[9] R. Morphy, C. Kay, Z. Rankovic, From magic bullets to designed multiple ligands, Drug Discov. Today 9 (2004) 641–651.
[10] J. Walsh, A. Bell, Hybrid drugs for malaria, Curr. Pharmaceut. Des. 15 (2009) 2970–2985.
[11] J.J. Walsh, D. Coughlan, N. Heneghan, C. Gaynor, A. Bell, A novel artemisinin-quinine hybrid with potent antimalarial activity, Bioorg. Med. Chem. Lett 17 (2007) 3599–3602.
[12] F.W. Muregi, A. Ishih, Next-Generation antimalarial drugs: hybrid molecules as a new strategy in drug design, Drug Dev. Res. 71 (2010) 20–32.
[13] R. Oliveira, D. Miranda, J. Magalhães, R. Capela, M.J. Perry, P.M. O'Neill, R. Moreira, F. Lopes, From hybrid compounds to targeted drug delivery in antimalarial therapy, Bioorg. Med. Chem. 23 (2015) 5120–5130.
[14] S. Vandekerckhove, M. D'hooghe, Quinoline-based antimalarial hybrid compounds, Bioorg. Med. Chem. 23 (2015) 5098–5119.
[15] M. Patra, G. Gasser, The medicinal chemistry of ferrocene and its derivatives, Nat. Rev. Chem. 1 (2017), 0066.
[16] https://clinicaltrials.gov/ct2/show/NCT03660839, 2019.
[17] F. Bellot, F. Cosledan, L. Vendier, J. Brocard, B. Meunier, A. Robert, Trioxaferroquines as new hybrid antimalarial drugs, J. Med. Chem. 53 (2010) 4103–4109.
[18] P. Chellan, V.M. Avery, S. Duffy, J.A. Triccas, G. Nagalingam, C. Tam, L.W. Cheng, J. Liu, K.M. Land, G.J. Clarkson, Organometallic conjugates of the drug sulfadoxine for combatting antimicrobial resistance, Chem. Eur J. 24 (2018) 10078–10090.
[19] N. Baartzes, T. Stringer, G.S. Smith, Targeting sensitive-strain and resistant-strain malaria parasites through a metal-based approach, in: Advances in Bioorganometallic Chemistry, Elsevier, 2019, pp. 193–213.
[20] T. Stringer, D. Taylor, H. Guzgay, A. Shokar, A. Au, P.J. Smith, D.T. Hendricks, K.M. Land, T.J. Egan, G.S. Smith, Polyamine quinoline rhodium complexes: synthesis and pharmacological evaluation as antiparasitic agents against *Plasmodium falciparum* and *Trichomonas vaginalis*, Dalton Trans. 44 (2015) 14906–14917.
[21] E. Ekengard, L. Glans, I. Cassells, T. Fogeron, P. Govender, T. Stringer, P. Chellan, G.C. Lisensky, W.H. Hersh, I. Doverbratt, Antimalarial activity of ruthenium (II) and osmium (II) arene complexes with mono-and bidentate chloroquine analogue ligands, Dalton Trans. 44 (2015) 19314–19329.
[22] T. Stringer, M.A.S. Quintero, L. Wiesner, G.S. Smith, E. Nordlander, Evaluation of PTA-derived ruthenium (II) and iridium (III) quinoline complexes against chloroquine-sensitive and resistant strains of the *Plasmodium falciparum* malaria parasite, J. Inorg. Biochem. 191 (2019) 164–173.
[23] M. Adams, C. de Kock, P.J. Smith, K. Chibale, G.S. Smith, Evaluation of ferrocenyl-containing benzothiazoles as potential antiplasmodial agents, Eur. J. Inorg. Chem. (2017) 242–246, 2017.
[24] L. Rylands, A. Welsh, K. Maepa, T. Stringer, D. Taylor, K. Chibale, G.S. Smith, Structure-activity relationship studies of antiplasmodial cyclometallated ruthenium (II), rhodium (III) and iridium (III) complexes of 2-phenylbenzimidazoles, Eur. J. Med. Chem. 161 (2019) 11–21.
[25] N. Baartzes, T. Stringer, R. Seldon, D. Warner, D. Taylor, S. Wittlin, K. Chibale, G. Smith, Bioisosteric ferrocenyl aminoquinoline-benzimidazole hybrids: antimicrobial evaluation and mechanistic insights, Eur. J. Med. Chem. 180 (2019) 121–133.
[26] A.R. Burgoyne, B.C. Makhubela, M. Meyer, G.S. Smith, Trinuclear half-sandwich RuII, RhIII and IrIII polyester organometallic complexes: synthesis and *in vitro* evaluation as antitumor agents, Eur. J. Inorg. Chem. (2015) 1433–1444, 2015.
[27] P. Govender, A.K. Renfrew, C.M. Clavel, P.J. Dyson, B. Therrien, G.S. Smith, Antiproliferative activity of chelating N, O-and N, N-ruthenium (II) arene functionalised poly (propyleneimine) dendrimer scaffolds, Dalton Trans. 40 (2011) 1158–1167.
[28] G. Gupta, B. Therrien, K.M. Rao, Half sandwich platinum group metal complexes containing tetradentate N-donor ligand bearing two pyrazolyl-pyridine units linked by an aromatic spacer, J. Organomet. Chem. 695 (2010) 753–759.
[29] M. Makler, J. Ries, J. Williams, J. Bancroft, R. Piper, B. Gibbins, D. Hinrichs, Parasite lactate dehydrogenase as an assay for *Plasmodium falciparum* drug sensitivity, Am. J. Trop. Med. Hyg. 48 (1993) 739–741.
[30] T. Mosmann, Rapid colorimetric assay for cellular growth and survival: application to proliferation and cytotoxicity assays, J. Immunol. Methods 65 (1983) 55–63.
[31] J. Carmichael, W.G. DeGraff, A.F. Gazdar, J.D. Minna, J.B. Mitchell, Evaluation of a tetrazolium-based semiautomated colorimetric assay: assessment of chemosensitivity testing, Canc. Res. 47 (1987) 936–942.
[32] R.D. Sandlin, M.D. Carter, P.J. Lee, J.M. Auschwitz, S.E. Leed, J.D. Johnson, D.W. Wright, Use of the NP-40 detergent-mediated assay in discovery of inhibitors of β-hematin crystallization, Antimicrob. Agents Chemother. 55 (2011) 3363–3369.
[33] K.K. Ncokazi, T.J. Egan, A colorimetric high-throughput β-hematin inhibition screening assay for use in the search for antimalarial compounds, Anal. Biochem. 338 (2005) 306–319.
[34] E. Ekengard, I. Bergare, J. Hansson, I. Doverbratt, M. Monari, B. Gordhan, B. Kana, C.d. Kock, P.J. Smith, E. Nordlander, A pyrazine amide-4-aminoquinoline hybrid and its rhodium and iridium pentamethylcyclopentadienyl complexes; evaluation of anti-mycobacterial and anti-plasmodial activities, J. Mex. Chem. Soc. 61 (2017) 158–166.
[35] J. Jorgensen, J. Turnidge, Susceptibility test methods: 211 dilution and disk diffusion methods, in: Manual of Clinical Microbiology, eleventh ed., American Society of Microbiology, 2015, pp. 1253–1273.
[36] R.C. Goldman, Why are membrane targets discovered by phenotypic screens and genome sequencing in *Mycobacterium tuberculosis*? Tuberculosis 93 (2013) 569–588.
[37] V. Makarov, B. Lechartier, M. Zhang, J. Neres, A.M. van der Sar, S.A. Raadsen, R.C. Hartkoorn, O.B. Ryabova, A. Vocat, L.A. Decosterd, Towards a new combination therapy for tuberculosis with next generation benzothiazinones, EMBO Mol. Med. 6 (2014) 372–383.
[38] G. Piccaro, G. Poce, M. Biava, F. Giannoni, L. Fattorini, Activity of lipophilic and hydrophilic drugs against dormant and replicating *Mycobacterium tuberculosis*, J. Antibiot. 68 (2015) 711.
[39] C. White, A. Yates, P. Maitlis, D. Heinekey, (η5-Pentamethylcyclopentadienyl) rhodium and-iridium compounds, Inorg. Synth. (1992) 228–234.
[40] SAINT Version 7.60a, Bruker AXS Inc., Madison, WI, USA, 2006.
[41] G.M. Sheldrick, SHELXL-2018/3 and SADABS Version 2.05, University of Göttingen, Germany, 1997.
[42] L.J. Barbour, X-Seed—a software tool for supramolecular crystallography, J. Supramol. Chem. Elsevier 1 (2001) 189–191.
[43] J.L. Atwood, L.J. Barbour, Molecular graphics: from science to art, Cryst. Growth Des. 3 (2003) 3–8.
[44] http://www.povray.org, 2019.
[45] W. Trager, J.B. Jensen, Human malaria parasites in continuous culture, Science 193 (1976) 673–675.
[46] J.H. Jorgensen, J.D. Turnidge, Susceptibility test methods: dilution and disk diffusion methods, in: Manual of Clinical Microbiology, eleventh ed., American Society of Microbiology, 2015, pp. 1253–1273.
[47] T.R. Ioerger, Y. Feng, K. Ganesula, X. Chen, K.M. Dobos, S. Fortune, W.R. Jacobs, V. Mizrahi, T. Parish, E. Rubin, Variation among genome sequences of H37Rv strains of *Mycobacterium tuberculosis* from multiple laboratories, J. Bacteriol. 192 (2010) 3645–3653.
[48] S.G. Franzblau, M.A. DeGroote, S.H. Cho, K. Andries, E. Nuermberger, I.M. Orme, K. Mdluli, I. Angulo-Barturen, T. Dick, V. Dartois, Comprehensive analysis of methods used for the evaluation of compounds against Mycobacterium tuberculosis, Tuberculosis 92 (2012) 453–488.
[49] Y.J. Tang, W. Shui, S. Myers, X. Feng, C. Bertozzi, J.D. Keasling, Central metabolism in Mycobacterium smegmatis during the transition from O2-rich to O2-poor conditions as studied by isotopomer-assisted metabolite analysis, Biotechnol. Lett. 31 (2009) 1233–1240.
[50] J. Ollinger, M.A. Bailey, G.C. Moraski, A. Casey, S. Florio, T. Alling, M.J. Miller, T. Parish, A dual read-out assay to evaluate the potency of compounds active against Mycobacterium tuberculosis, PloS one 8 (2013) e60531.
[51] The collaborative drug discovery database. www.collaborativedrug.com, 2018-2019.